Journal of Catalysis 279 (2011) 366–380

Contents lists available at ScienceDirect

Journal of Catalysis

journal homepage: www.elsevier.com/locate/jcat

Acidic and catalytic properties of hierarchical zeolites and hybrid ordered mesoporous materials assembled from MFI protozeolitic units

D.P. Serrano [a,c,*], R.A. García [b], G. Vicente [a], M. Linares [a], D. Procházková [d], J. Čejka [d,*]

[a] Chemical and Energy Technology Department, ESCET, Rey Juan Carlos University, c/Tulipán s/n, 28933 Móstoles, Madrid, Spain
[b] Chemical and Environmental Technology Department, ESCET, Rey Juan Carlos University, c/Tulipán s/n, 28933 Móstoles, Madrid, Spain
[c] IMDEA Energy Institute, c/Tulipán s/n, 28933 Móstoles, Madrid, Spain
[d] J. Heyrovský Institute of Physical Chemistry, Academy of Sciences of the Czech Republic, v.v.i., Dolejškova 3, CZ-182 23 Prague 8, Czech Republic

ARTICLE INFO

Article history:
Received 12 November 2010
Revised 17 February 2011
Accepted 17 February 2011
Available online 21 March 2011

Keywords:
Hierarchical zeolites
Hybrid zeolitic-mesostructured materials
Brønsted and Lewis acid centres
Epoxide rearrangement
Friedel–Crafts acylation

ABSTRACT

Two types of MFI zeolitic materials with improved accessibility, hierarchical zeolites and hybrid ordered mesoporous materials are here compared in terms of textural, acidic and catalytic properties. In both cases, protozeolitic units were employed as starting building blocks, the growth of which was perturbed by a silanization agent (hierarchical ZSM-5) or controlled by assembling around surfactant micelles (hybrid ordered mesoporous material, HZM). Likewise, two standard samples (nanocrystalline ZSM-5 and Al-MCM-41) were used as reference. Nitrogen adsorption measurements confirmed the presence of a secondary porosity and a high share of non-microporous surface area in hierarchical ZSM-5, whereas no significant amount of micropores was detected in the hybrid HZM sample. However, ^{27}Al MAS NMR measurements indicated that zeolitic fragments are present within the walls of the latter sample. The acidic properties of the materials under study were extensively investigated by adsorption–desorption of different base probe molecules. Specifically, FTIR spectra taken after pyridine adsorption show the presence of a high population of strong Lewis acid sites in both hierarchical ZSM-5 and HZM samples. This fact, along with a high accessibility to the active sites, is proposed to be mainly responsible for the enhanced catalytic activity exhibited by these materials in 1,2-epoxyoctane rearrangement and anisole acylation. The results obtained clearly indicate the strong and positive influence of the textural and acidic features of the hierarchical materials on their catalytic properties.

1. Introduction

Zeolites are well-known crystalline microporous materials widely used as heterogeneous catalysts and adsorbents in a variety of fields, like oil refining, petrochemistry and the fine chemical industry. However, as a result of their small pore size, significant drawbacks are associated with them in applications involving large compounds. Thus, zeolites may experience diffusion limitations, related to the intracrystalline transport of the reactants to reach the active sites and of products to move away from these sites [1]. In addition, in most reactions, coke formation enhances these limitations, as the coke deposits block the zeolite micropores, causing a rapid drop in the catalytic activity. On the other hand, bulky compounds cannot access in many cases the internal surface area of the zeolites, which restricts their use as catalysts in important chemical processes.

The synthetic effort for developing materials with large and well-defined pores resulted in the successful synthesis of ordered mesoporous materials, which possess uniform mesopores that can be varied in a wide range [2–4]. Unfortunately, the amorphous walls of these materials were not able to match the stability, acid strength and catalytic activity typically associated with crystalline zeolites. Accordingly, in recent years, much research work and great attention have been devoted to overcome the limitations of both types of materials by trying to combine the advantages of zeolites and benefits from ordered mesoporous materials [5].

One of the synthetic approaches followed by many research groups with that objective has led to the development of hierarchical zeolites, i.e. zeolitic materials possessing a secondary porosity, usually in the mesopore range, in addition to the typical zeolite micropores. The presence of the secondary porosity has been reported to cause positive effects as it increases the accessibility of the zeolite active sites, solving and/or lowering the diffusion and steric constraints found in conventional zeolites. The methods employed for the preparation of hierarchical zeolites include hard templating routes [6], the use of organosilane surfactants or polymers as soft templates [7,8], packing of nanosized zeolite crystals

* Corresponding authors.
E-mail addresses: david.serrano@urjc.es (D.P. Serrano), jiri.cejka@jh-inst.cas.cz (J. Čejka).

0021-9517/$ - see front matter © 2011 Elsevier Inc. All rights reserved.
doi:10.1016/j.jcat.2011.02.007

[9], demetallation of zeolites for the post-synthetic generation of mesopores [10], the simultaneous crystallization of precursor phases of both zeolite and ordered mesoporous [11], the pseudomorphic transformation of porous silica gel [12], etc.

Another strategy for developing zeolitic materials with improved accessibility to the active sites is based on the generation of zeolitic entities or fragments within the walls of ordered mesoporous materials, such as MCM-41 and SBA-15. These materials could be considered as hybrid solids of zeolites and ordered mesoporous materials. The first attempts in this direction tried to provoke a crystallization of the amorphous walls of the ordered mesoporous materials by a post-synthesis treatment under the presence of the appropriate zeolite structure-directing agent. However, this route usually led to phase segregation with large zeolite crystals emerging from the mesoporous material. More successful has been the method starting from zeolitic seeds, which were further organized by surfactant micelles to yield mesostructured solids having zeolitic seeds embedded within the mesopore walls. The hybrid materials so obtained, although being X-ray amorphous, show enhanced stability and catalytic activity in a variety of reactions compared with both conventional zeolites and ordered mesoporous aluminosilicates.

Independently of the method employed to synthesize zeolitic materials with improved accessibility, some of the most critical factors controlling their catalytic behaviour are the sharing of active sites between the internal and external surfaces and the strength and nature of their acid sites. It is well known that zeolite acidity is associated with the presence of aluminium or other trivalent cations in the silica framework creating a negative charge in the structure. The strength and nature of the acid sites in zeolites is a complex issue influenced by a variety of factors: crystalline structure, Si/Al ratio, defect concentration, previous thermal treatments, etc. Two types of acid sites are typically present in zeolites: Brønsted-type acidity attributed to the protons connected to the Si–O–Al linkages and Lewis-type acidity associated with the presence of electron-acceptor aluminium species. The estimation of the acid strength and concentration of acid centres in zeolitic materials is essential to completely understand their catalytic behaviour [13]. This is even more important in the case of hierarchical zeolites and hybrid zeolitic materials, since the presence of a large part of the acid sites outside the zeolite micropores is expected to induce great changes in their acid features and therefore in their catalytic behaviour.

The acidity of zeolites is usually characterized by interaction with probe molecules, possessing different basic function and being able to distinguish different types of acid sites present on the zeolite surface. FTIR spectroscopy of adsorbed molecules is one of most common methods applied to investigate the acid sites of zeolite catalysts, whereas ammonia and pyridine are typical probe molecules employed to study their nature, distinguishing between different sites and strengths [14–16].

While an increasing number of works are published every year dealing with hierarchical zeolites or hybrid zeolitic-ordered mesoporous solids [17], almost none has so far reported comparing both types of materials. Accordingly, the current work has been outlined to compare the physicochemical properties and the catalytic activity of both classes of zeolitic materials using the same zeolite structure (MFI topology), techniques, conditions and reaction tests.

The method here employed for the preparation of hierarchical zeolites is based on the crystallization of silanized protozeolitic units. The incorporation of the seed silanization agent (SSA) hinders the growth of the zeolite crystals and prevents their further aggregation. The materials obtained applying this strategy show high non-microporous surface area, as they consist of ultra-small zeolite nanounits with an additional porosity in the supermicro-mesopore regions generated by the silanization agents. This method has been successfully applied to obtain, among others, ZSM-5, ZSM-11 and beta zeolites with hierarchical porosity. These materials showed a better catalytic activity in different reactions involving bulky molecules than the reference zeolite samples [18,19]. On the other hand, hybrid zeolitic-ordered mesoporous materials have been prepared in this work by the assembly of protozeolitic units around surfactant micelles [20–22].

The controlled generation of mesoporosity and high non-microporous surface area in modified zeolites deserves a particular attention since it is necessary to determine the specific nature and location of their acid sites. In this way, the distribution of active sites between the external and internal zeolite surfaces can be studied by adsorbing bulky probe molecules, unable to enter into the zeolitic micropores [23]. Thus, a number of works have been reported to measure the different location and accessibility of the zeolite acid sites using a variety of probe molecules, such as allyl 3,5-di-tert-butyl ether to study MOR and BEA zeolites [24], 2,6-lutidine and 2,4,6-collidine over MFI materials [25], and acetonitrile, pivalonitrile and 2,6-di-tert-butylpyridine over different structures [26,27]. In this contribution, FTIR spectroscopy of adsorbed pyridine, d_3-acetonitrile and 2,6-di-tert-butyl pyridine (DTBP) has been used to quantitatively determine the changes in the concentration of internal and externally accessible acid sites of the materials prepared by both strategies followed in this work: the development of hierarchical zeolites and the synthesis of hybrid mesostructured zeolitic materials. In addition, structural factors like crystallinity and ordering, as well as surface area and pore size distribution have been conveniently ascertained for both types of zeolitic materials using different techniques.

The variety of pore topologies and pore sizes within the hierarchical zeolite and hybrid zeolitic-mesoporous materials, along with the possibility to tune their acidity, and to regenerate them, make these materials attractive heterogeneous catalysts for different reactions involving bulky molecules, as epoxide rearrangement reactions and Friedel–Crafts acylation. The first one is a process of high interest to synthesize a variety of organic compounds, such as aldehydes, ketones, ethers and alcohols, which are utilized as intermediates or final products in fine chemical reactions [28]. Heterogeneous catalysts such as SiO_2, Al_2O_3, ZnO, supported metals and a variety of precipitated phosphates have been tested for epoxide rearrangement reactions. However, use of these conventional catalysts often results in the formation of aldol condensation products and mixtures of ketones and aldehydes as by-products. [29]. In contrast, zeoltic materials have shown several advantages, since their uniform acid strength and shape selectivity may reduce the above-mentioned side reactions, although limited by diffusional and steric constraints for the isomerisation of bulky epoxides [30].

On the other hand, acylation of aromatic compounds into ketones is a process of commercial relevance in the fine chemicals sector, particularly in the field of the pharmaceutical industries. It takes place by the reaction of an aromatic substrate with an acylating agent, such as acyl halides, acid anhydrides or esters, in the presence of an acid catalyst (usually $AlCl_3$, BF_3 or HF) [31]. Currently, economic and environmental factors demand the replacement of these corrosive systems by heterogeneous acid catalysts, such as zeolites, clays and heteropolyacids [32–36]. In particular, zeolites have shown promising results as acylation catalysts of different substrates [34,37].

The present work is aimed at the investigating performance of both hierarchical zeolites and hybrid zeolitic-mesoporous materials as catalysts for the 1,2-epoxyoctane isomerisation and anisole acylation, being compared with both conventional Al-MCM-41 and nanocrystalline ZSM-5 zeolite.

2. Experimental

2.1. Materials synthesis

2.1.1. Hierarchical zeolites

Hierarchical ZSM-5 zeolite was prepared, using tetrapropylammonium hydroxide (TPAOH) as structure-directing agent (SDA), from a solution having the molar composition: Al_2O_3:60 SiO_2:11 TPAOH:1500 H_2O [38]. The precursor solution was precrystallized in a round-bottomed flask equipped with a condenser under stirring at 90 °C for 20 h. Thereafter, the corresponding amount of phenylaminopropyl-trimethoxysilane (PHAPTMS) was added to the solution, being kept under reflux and stirring at 90 °C for 6 h. Two different hierarchical ZSM-5 samples (h-ZSM-5 (5%) and h-ZSM-5 (12%)) were prepared by adding the organosilane to the precrystallized solution in proportions of 5 and 12 mol%, respectively, related to the total silica content of the gel. The final crystallization of the functionalized protozeolitic units was carried out in Teflon-lined autoclave at 170 °C for 7 days. The solid products obtained from the synthesis were separated by centrifugation, washed out with distilled water, dried overnight at 110 °C and calcined in a stream of air at 550 °C for 5 h.

A reference ZSM-5 sample (ZSM-5 (0%) was synthesized using the same procedure without the silanization step.

2.1.2. Hybrid zeolitic-ordered mesoporous materials

Protozeolitic units, obtained in the early stages of ZSM-5 crystallization, were assembled around cetyltrimethylammonium bromide (CTAB) micelles to obtain hybrid zeolitic-ordered mesoporous materials (HZM). Thereby, a ZSM-5 synthesis gel was prepared according to a procedure earlier reported [38]. The gel was aged for 40 h at room temperature in order to promote the generation of the zeolite seeds and then crystallized at 90 °C. Then, the formation of the mesostructure was achieved by the addition of both the surfactant (CTAB) and water to the zeolite seed solution, a mixture with the following molar composition being obtained: Al_2O_3:60 SiO_2:11 TPAOH:15 CTAB:2400 H_2O. After an additional ageing period of 4 h at room temperature, the mixture was transferred into an autoclave and heated at 110 °C for 2 days under static conditions. The solid product finally obtained was separated by centrifugation, washed with distilled water, dried overnight at 110 °C and calcined in air at 550 °C for 5 h.

On the other hand, a sample of conventional Al-MCM-41 was also synthesized according to procedures published in literature in order to have a reference material for ordered mesoporous material [39].

2.2. Characterization

XRD patterns of the different samples were obtained with a Philips ŹPERT MPD diffractometer using Cu Kα radiation. Both low- and wide-angle X-ray patterns were collected in order to characterize the mesoscopic ordering and the zeolite crystallinity of the samples, respectively.

Nitrogen adsorption–desorption isotherms at −196 °C of the calcined catalysts were measured with a Micromeritics TRISTAR 3000 instrument. Argon adsorption–desorption isotherms at −186 °C were also recorded for the zeolite samples using an Autosorb instrument (Quantachrome). Prior to the measurements, the individual samples were outgassed at 300 °C under vacuum. The surface area was determined applying the Brunauer–Emmet–Teller (BET) equation. The pore size distributions were calculated using the adsorption branch of the argon isotherms by applying the NLDFT model (Quantachrome).

The Si/Al atomic ratio of the samples was determined by ICP-AES measurements with a Varian VISTA-AX-CCD equipment. TEM images were obtained in a PHILIPS TECHNAI 20 electron microscope operating at 200 kV. Ammonia temperature-programmed desorption (TPD) experiments were carried out in a Micromeritics 2910 (TPD/TPR) equipment.

The acidic properties of the samples were investigated by the adsorption of pyridine and d_3-acetonitrile, used as probe molecules, followed by FTIR spectroscopy. All samples were prepared as self-supporting wafers (ca. 8–12 mg/cm^2) and activated overnight at 450 °C under vacuum prior to the adsorption of the probe molecules. Adsorption of probe molecules was investigated on a Nicolet Protégé 460 spectrometer with a resolution of 4 cm^{-1}. Pyridine was adsorbed at 150 °C, while d_3-acetonitrile at room temperature. FTIR spectra of adsorbed probe molecules were recorded after 30 min of desorption. All measured spectra were recalculated to a "normalized" wafer of 10 mg/cm^2. For a quantitative characterization of acid sites, the following bands and absorption coefficient were used: pyridine PyH^+ band at 1545 cm^{-1}, ε = 1.67 cm μmol^{-1}, pyridine PyL bands at 1461 + 1454 cm^{-1}, ε = 2.2 cm μmol^{-1}, d^3-acetonitrile Brønsted band at 2296 cm^{-1}, ε = 2.05 cm μmol^{-1}, acetonitrile strong and weak Lewis bands at 2323 and 2310 cm^{-1}, ε = 3.60 cm μmol^{-1} [14].

In addition, adsorption of 2,6-di-tert-butyl pyridine was studied to distinguish between acid sites located on the external surface of zeolite crystals and the overall concentration of these sites. For that purpose, adsorption of 2,6-di-tert-butyl pyridine (degassed by repeated cooling and thawing cycles) proceeded at 150 °C by equilibrating the zeolite wafer with the probe vapour pressure for 15 min followed by 1 h degassing at the same temperature and by collection of the spectrum at room temperature.

2.3. Catalytic tests

The catalytic experiments of 1,2-epoxyoctane isomerisation were carried out in a 0.1-L stirred batch autoclave, equipped with a temperature controller and a pressure gauge under stirring (550 rpm) and autogeneous pressure. This experimental set-up was also provided with a device to feed the epoxide into the Teflon-lined reactor once the reaction temperature was reached. The catalyst was previously dried overnight at 135 °C and then transferred to the reactor with toluene (47 g), used as solvent, starting the stirring and heating of the mixture. The zero time of the reaction is taken when the temperature reaches the set-point value (150 °C) and the substrate, 1,2-epoxyoctane (1.25 g), is added to the reactor (catalyst/epoxide = 0.08 w/w) [30]. Periodically, aliquots of the reaction mixture were collected in order to assess the evolution of the reaction, the mixture being allowed to react for 120 min.

The reaction products were analysed with a VARIAN 3800 gas chromatograph equipped with a capillary column (HPFFAP) with dimensions 60 × 0.32 mm, using a flame ionization detector. Identification of the different reaction products was performed by mass spectrometry (VARIAN SATURN 2000) using standard compounds.

The catalytic tests of anisole acylation were carried out under atmospheric pressure in a 250-ml three-necked batch reactor equipped with a reflux condenser, a thermometer and a magnetic stirrer. A typical reaction was carried out as follows: 5.46 g (50 mmol) of anisole in 50 ml of solvent (nitrobenzene) was introduced into the reactor. Subsequently, 1 g of sulpholane, used as internal standard, and 50 mmol of acylating agent (acetyl chloride) were added to the reaction mixture. The latter was kept magnetically stirred under nitrogen stream. Once the reaction temperature (120 °C) was reached, 0.273 g of fresh catalyst (catalyst/anisole = 0.05 w/w) was added to the flask [40]. Periodically, aliquots of the reaction mixture were collected in order to assess the time

evolution of the reaction, the mixture being allowed to react for 180 min. The products were analysed by capillary gas chromatography in a Varian 3900 Series instrument equipped with a 30 m × 0.25 mm capillary column (CP SIL 8 CB) and a FID detector.

3. Results and discussion

3.1. Crystallinity and ordering

Five different materials have been prepared and investigated in this work. These include two hierarchical ZSM-5 samples (h-ZSM-5), one hybrid zeolitic-ordered mesoporous material (HZM) and two reference samples (nanocrystalline ZSM-5 and Al-MCM-41). The two h-ZSM-5 samples, h-ZSM-5 (5%) and h-ZSM-5 (12%), have been prepared varying the proportion of the silanization agent (5% and 12% referred to the total silica content of the gel). They were expected to show a different distribution of the hierarchical porosity between micro- and mesopores. Likewise, the ZSM-5 reference sample, ZSM-5 (0%), has been obtained using the same synthesis conditions as for the latter but omitting the seed silanization treatment. Regarding the ordered mesoporous materials, a precrystallization step was carried out in the synthesis of the HZM sample to form protozeolitic units before the addition of the surfactant. This step was omitted in the preparation of the Al-MCM-41 reference sample.

Fig. 1a compares wide-angle XRD patterns of these materials. Sample ZSM-5 (0%) shows the typical diffractogram corresponding to the MFI zeolite structure. The intensity of the X-ray diffraction lines decreases in the case of the hierarchical ZSM-5 samples, especially as the amount of PHAPTMS introduced in the seed silanization step is increased. According to the Scherrer law for powder XRD, the increase in the peak width, measured at half height, is indicative of a reduction in the crystal size. Therefore, a decrease in the size of the crystalline domains is produced with the incorporation of the seed silanization agent (SSA). In the case of the ordered mesoporous materials, no diffraction lines are observed in the wide-angle region for the Al-MCM-41 sample. This result was expected due to the amorphous nature of its pore walls. The same occurs for the hybrid material, in spite of being synthesized from protozeolitic units. Taking into account that the width of its pore walls is around 1 nm, the crystalline fragments located inside them are too small to be distinguished by X-ray diffraction. Likewise, no diffraction lines coming from other aluminium compounds, such as crystalline alumina and aluminium oxyhydroxide species, are observed. On the other hand, in the low-angle XRD patterns (Fig. 1b), an intense peak is present for both Al-MCM-41 and HZM, confirming these materials exhibit mesoscopic order. However, no additional secondary peaks are detected at higher angles, in contrast to the case of pure silica MCM-41. It is well known that the introduction of aluminium causes a decrease in the regularity of the mesopore array leading to materials with lower long-range mesoscopic order [39]. The low-angle diffraction line is absent in the case of the zeolite samples as they do not show any mesostructure. For the HZM sample, the diffraction peak is shifted towards lower angles, i.e. larger d-spacing, compared with Al-MCM-41.

Fig. 2 illustrates TEM images corresponding to the individual samples with different levels of resolution. The reference ZSM-5 (0%) is formed by nanocrystals with sizes in the range 40–80 nm, i.e. it can be considered a nanocrystalline ZSM-5 sample. A completely different morphology is observed for the hierarchical ZSM-5 samples. They consist of aggregates, with a size in the range 400–600 nm. The latter are really formed by very small entities, having sizes below 10 nm (nanounits). Thus, in the border of the aggregates, nanounits with sizes as small as 5 nm can be denoted for both hierarchical ZSM-5 materials. Moreover, in spite of their really low size, the presence of diffraction lines over the nanounits is clearly observed in the images taken at high magnifications (see Figs. S1 and S2 in Supporting information). This result confirms the high crystallinity of these samples. In addition, high-resolution TEM images indicate that adjacent nanounits show the same orientation of the crystallographic planes evidencing a significant degree of intergrowth among them. This fact is very important as it imparts identity and stability to the nanounit aggregates. Moreover, it explains why these samples exhibit X-ray crystallinity in spite of the low size of the nanounits (the crystalline domains are quite larger than a single nanounit). In the case of Al-MCM-41, the TEM image shows areas with hexagonal array of mesopores typically observed in this type of materials. In contrast, the HZM sample exhibits a wormhole mesopore arrangement, indicating

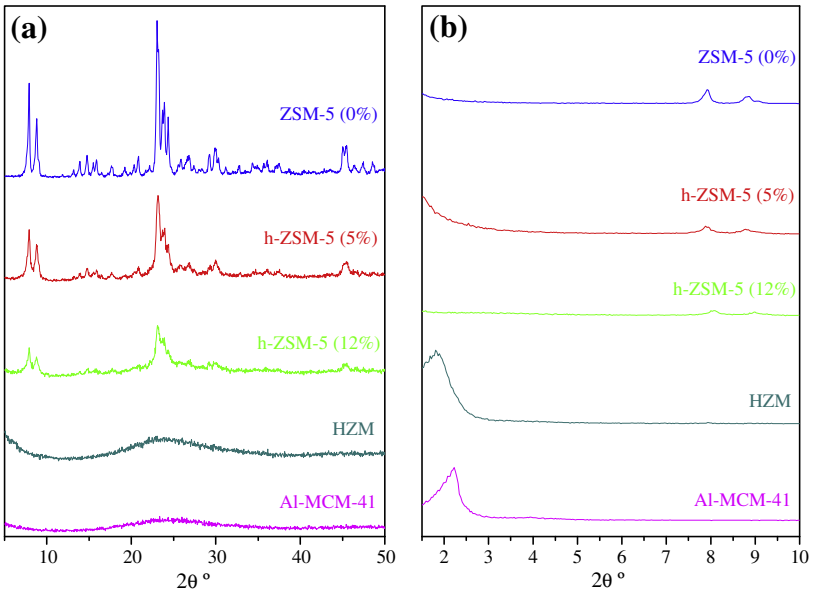

Fig. 1. XRD patterns of the calcined samples: (a) wide-angle region, (b) low-angle region.

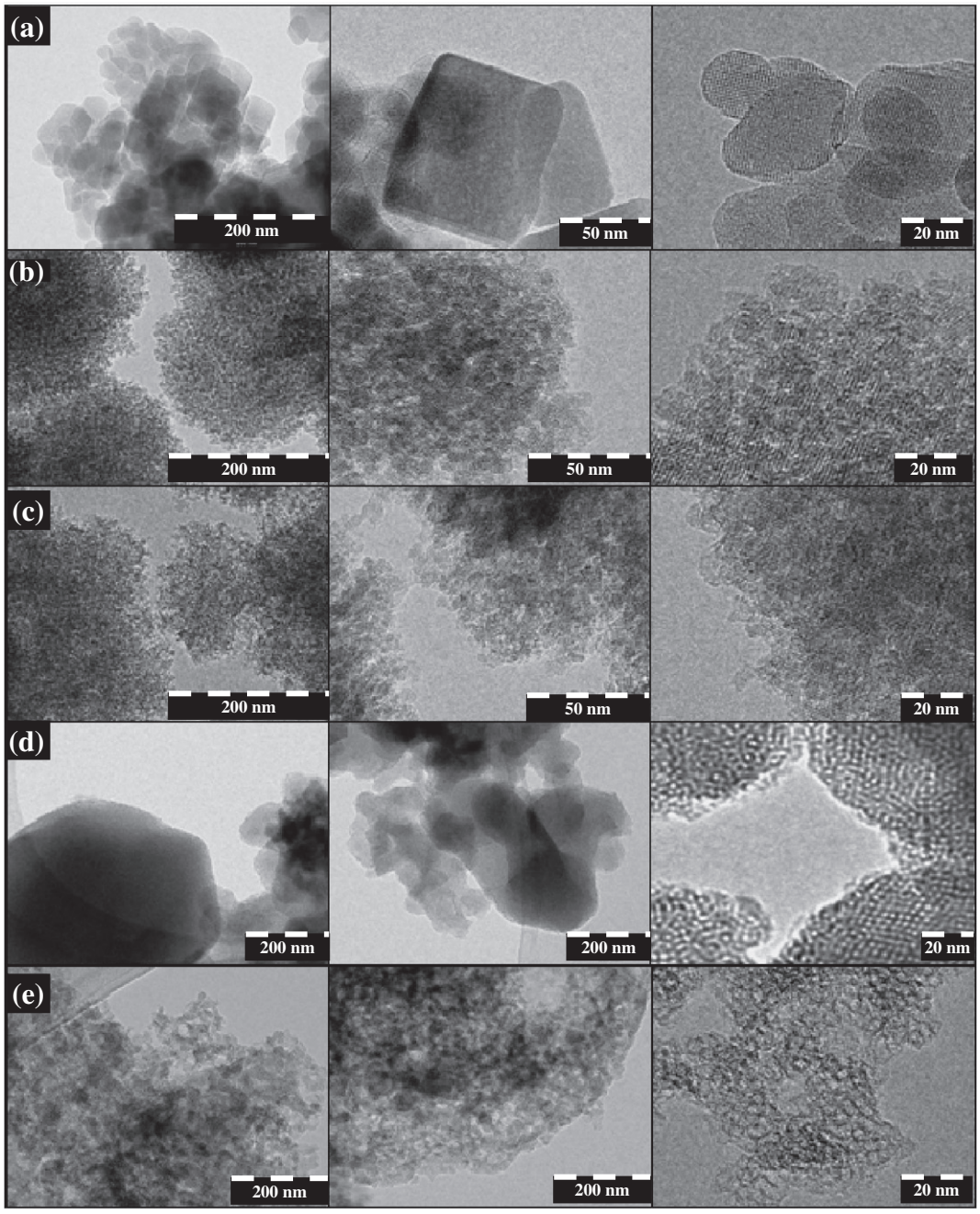

Fig. 2. TEM images of samples: (a) ZSM-5 (0%), (b) h-ZSM-5 (5%), (c) h-ZSM-5 (12%), (d) Al-MCM-41, (e) HZM.

that it possesses a lower long-range ordering than Al-MCM-41. This could be an evidence of the presence of zeolitic fragments within the HZM walls, as they are expected to cause a distortion of the mesoscopic order. Moreover, the particles of the HZM samples are not completely compact, which leads to the appearance of large voids, in addition to the mesopores, with sizes varying in a wide range (10–40 nm).

3.2. Textural properties

The textural properties of the samples were investigated by gas adsorption measurements. Fig. 3 shows the N_2 adsorption–desorption isotherms corresponding to the ordered mesoporous materials. The Al-MCM-41 isotherm is typical of well-synthesized ordered mesoporous materials with a steep increase in the adsorbed amount at a relative pressure of about 0.32 caused by the mesopore filling. As shown in Table 1, both ordered mesoporous materials present high BET surface area (893 and 976 m^2/g, respectively), with a value clearly larger for the hybrid sample. The BJH pore size distribution confirms that Al-MCM-41 possesses well-defined mesopores. The isotherm of the HZM sample presents at low relative pressures the same shape as that of Al-MCM-41. However, at high relative pressures, the HZM material exhibits an additional adsorption compared with Al-MCM-41. In this way, the pore size distribution of the HZM samples shows the presence of two types of mesoporosity. The first peak corresponds to that typical of ordered mesoporous materials, while the second one is quite less uniform and located in the range 10–40 nm. This could be at first assigned to interparticle porosity. However, the HZM particles are not very different in size from those of Al-MCM-41, while this

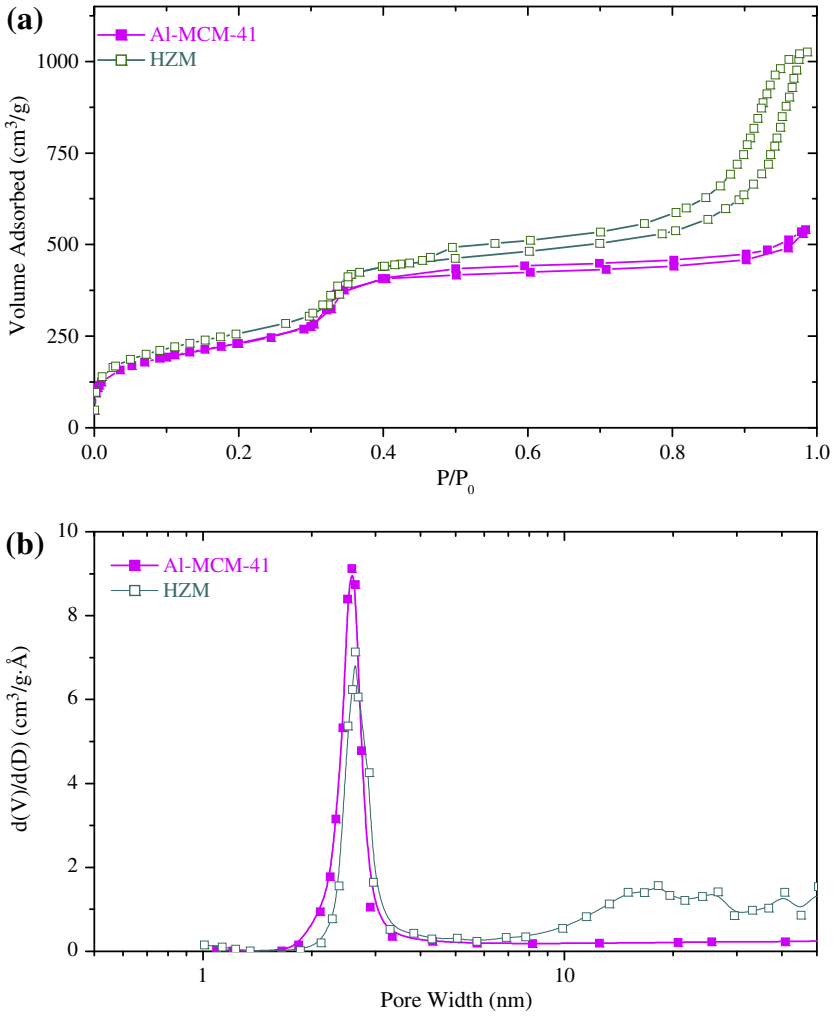

Fig. 3. N_2 adsorption–desorption at 77 K: (a) isotherms, (b) BJH pore size distributions.

Table 1
Physicochemical properties of the samples: ordered mesoporous materials (top), zeolites (bottom).

Sample	S_{BET}[a] (m^2/g)	$V_{\mu p}$[b] (cm^3/g)	D_p (nm)	T_{max}[c] (°C)	Acid sites[c] (mmol/g)	Si/Al[d]
Al-MCM-41	893	0	2.58	258	0.2012	28
HZM	976	0.006	2.62	259	0.2671	29
Sample	S_{BET}[e] (m^2/g)	S_{EXT}[f] (m^2/g)	$V_{\mu p}$[g] (cm^3/g)	T_{max}[c] (°C)	Acid sites[c] (mmol/g)	Si/Al[d]
ZSM-5 (0%)	431	78	0.1977	357	0.4259	31
h-ZSM-5 (5%)	524	261	0.1465	349	0.3660	32
h-ZSM-5 (12%)	696	456	0.1334	329	0.3303	34

[a] N_2 isotherm.
[b] t-plot.
[c] NH_3 TPD.
[d] ICP.
[e] Ar isotherm.
[f] SEXT – non-micropore surface area = SBET – $S_{\mu p}$.
[g] NLDFT.

peak is not present in the PSD of the latter. Moreover, as above commented, TEM images of the HZM sample denotes the presence also of large and irregular voids with sizes that match well with those obtained from the nitrogen adsorption isotherm for the additional mesoporosity.

In the case of the zeolitic samples, the textural properties have been determined from Ar adsorption–desorption measurements. The use of Ar instead of N_2 allows the pore size distribution to be obtained as a continuous curve for a wide range of pore sizes by employing the NLDFT model, as well as to distinguish the contribution of the different levels of porosity present in these samples to both the overall surface area and pore volume.

Fig. 4 shows that the Ar adsorption in the hierarchical ZSM-5 samples is strongly enhanced compared with the reference one. The isotherm of sample ZSM-5 (0%) is typical of microporous solids with a high adsorption at low relative pressures. In addition, it

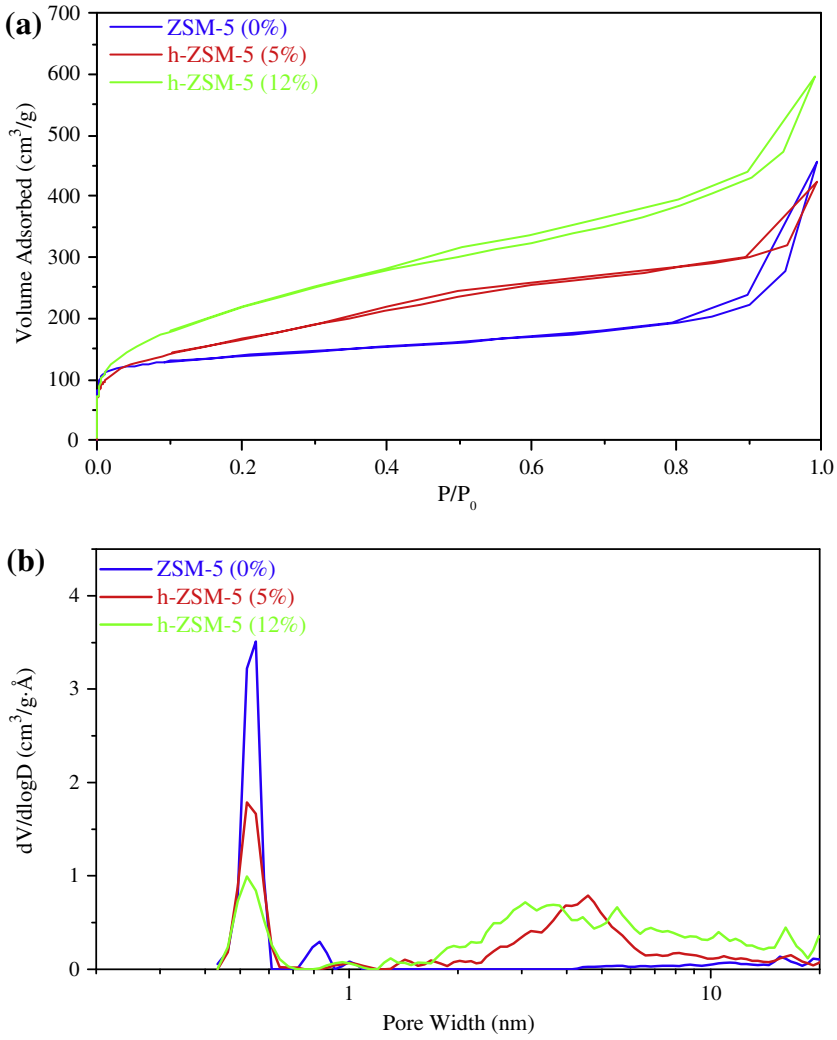

Fig. 4. Ar adsorption–desorption at 87 K: (a) isotherms, (b) NLDFT pore size distributions.

shows also a significant adsorption at high relative pressures, denoting the presence of intercrystalline porosity. This is consistent with the ZSM-5 (0%) sample being formed by nanocrystals in the 40–80 nm range. In the case of the hierarchical zeolites, the Ar adsorption takes place at both low and intermediate relative pressure. The latter is due to the presence of a secondary porosity associated with the voids existing among the individual nanounits, i.e. within the aggregates shown in Fig. 2. This is confirmed by the pore size distribution derived from the NLDFT model. In addition to the peak corresponding to the ZSM-5 micropores, the hierarchical samples possess a second peak placed in the range 2–8 nm. This peak is broader, and its contribution is larger, for the h-ZSM-5 (12%) sample, showing that a higher amount of SSA leads to a broader distribution of sizes for the secondary porosity.

The surface area (BET, micropore and external) of these samples, determined from the Ar isotherms, are summarized in Table 1. It must be noticed that the term "external surface area" is used here to refer to all the non-microporous surface area, including the adsorption in the different types of mesopores and on the outer surface of the particles. The enhanced adsorption exhibited by the hierarchical ZSM-5 samples is reflected also in their higher BET surface area compared with the reference ZSM-5. This fact has been earlier explained by a less-restricted gas adsorption taking place on the external and/or mesopore surface of zeolites regarding the expense of the adsorption within the micropores [18]. Although the external surface area of the ZSM-5 reference sample is quite large (78 m^2/g), due to its nanocrystalline character, this parameter is strongly increased for the hierarchical ZSM-5 materials reaching 456 m^2/g for h-ZSM-5 (12%). This effect is clearly dependent on the amount of SSA employed. Increasing the SSA proportion causes a progressive reduction in the micropore volume and an increase in the external surface area.

3.3. Aluminium state

As it is well known, the acidic properties of zeolitic materials and other aluminosilicates are related to the presence of Al species, which leads to the generation of both Brønsted and Lewis acid sites. Thereby, the different materials studied in this work were prepared with similar Al contents. The Si/Al ratio of the obtained samples varies in the range 28–34 (see Table 1), which is close in all cases to the Si/Al ratio corresponding to the synthesis gel.

The state, coordination, location and stability of these Al species have been investigated by ^{27}Al MAS NMR as illustrated in Fig. 5. In the case of the zeolites, the as-made materials exhibit just tetrahedral Al atoms, a single peak being observed in the spectra at around 50 ppm. Upon calcination, octahedrally coordinated aluminium, i.e. aluminium in non-framework positions, is also detected as demonstrated by the appearance of a characteristic peak at around 0 ppm. For the ZSM-5 (0%) sample, the contribution of this peak is

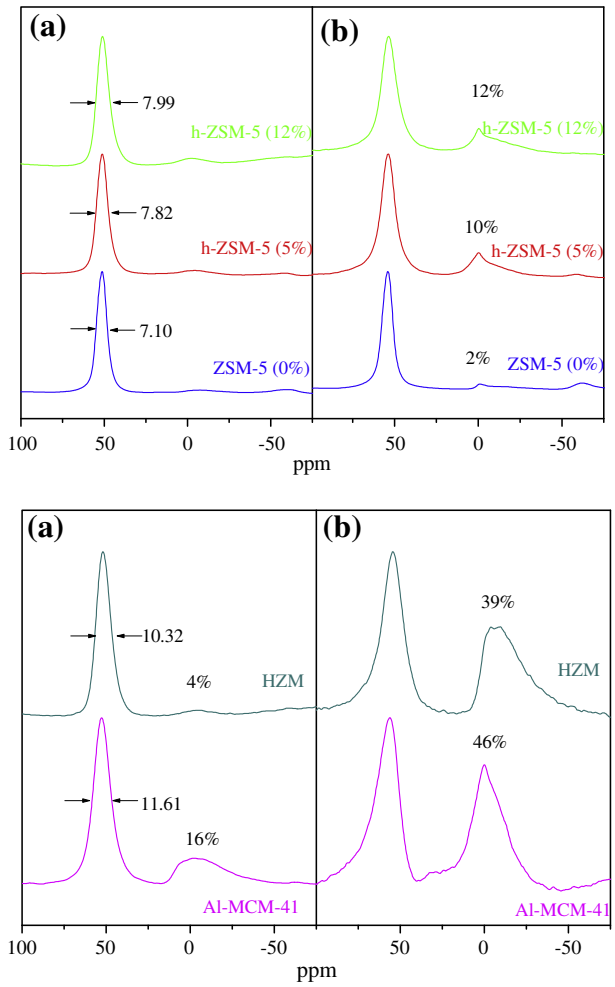

Fig. 5. ^{27}Al MAS NMR spectra of the samples: (a) as-synthesized, (b) after calcination.

almost negligible, whereas it reaches values of 10% and 12% for h-ZSM-5 (5%) and h-ZSM-5 (12%) materials. This result indicates a somewhat lower stability of the Al atoms in hierarchical zeolites compared with the reference sample. In contrast, the spectra of the ordered mesoporous materials, HZM and Al-MCM-41, show a noticeable amount of extra-framework aluminium even in the as-synthesized samples, which is strongly enhanced after calcination. In both cases (as-made and calcined samples), the proportion of non-framework octahedral aluminium is lower for the hybrid HZM sample than for Al-MCM-41, denoting a higher stability of the Al species in the former, which could be related to the presence of zeolitic entities within its walls.

On the other hand, the full-width-at-half-maximum (FWHM) values for tetrahedral Al peak of the as-made samples have been estimated from the ^{27}Al MAS NMR. This parameter provides a measurement of the uniformity of the Al environments in both zeolites and ordered mesoporous materials [41]. For the zeolites, the FWHM values increase in the range 7–8 ppm from the reference material to the hierarchical ZSM-5 samples. Among the latter, the FWHM is larger for the sample obtained using a higher amount of seed silanization agent. This fact clearly evidences that introducing a secondary porosity in ZSM-5 zeolite slightly decreases the uniformity of the Al environments, which is probably due to the features of the external surface as it provides a less-restricted environment. Both Si and Al atoms located on the external surface show a lower connectivity, since the latter is terminated by silanol groups, which means that a higher flexibility for them is expected in terms of bond lengths and angles. This fact is reflected in the less uniformity of the Al species detected in the MAS NMR measurements. In the case of the ordered mesoporous materials, significant differences are also observed in the FWHM values. Thus, Al-MCM-41 possesses a FWHM value (11.61 ppm) quite higher than those corresponding to the zeolites, which is consistent with the high variety of Al sites present in the amorphous walls of this material. Interestingly, the hybrid HZM exhibits a FWHM value (10.32 ppm) intermediate between those of zeolites and that of Al-MCM-41, although closer to that of the latter, which again can be taken as an indication of the presence of zeolitic units in this sample.

3.4. Acidic properties

Ammonia TPD is a widely applied method for characterizing the acidic properties of zeolites as it provides information on both the total number of acid sites (calculated from the NH_3 detected during desorption) and their acid strength (related to the temperature of the peak maximum in the desorption curve). The results obtained in the NH_3 TPD measurements in the present work are summarized in Table 1.

For the reference ZSM-5 sample, the total amount of acid sites quantified from the desorbed ammonia is in good agreement with its Al content (Si/Al = 31). It indicates that all the Al sites are accessible for ammonia molecules. However, for the rest of the samples, the concentrations of acid sites detected in the NH_3 TPD measurements are well below the theoretical value corresponding to their Si/Al ratios. In the case of the zeolite samples, a trend of decreasing the acid sites concentration is observed as the ratio external/micropore surface area is augmented. These discrepancies between the acid site concentrations from NH_3 TPD and from the Al content may be assigned to different reasons: presence of Al atoms in non-accessible positions or non-framework octahedral Al of the pore walls, existence of weak acid sites that undergo the NH_3 desorption during the physidesorption treatment of the ammonia TPD tests and changes in the type of acid sites present in the samples that exhibit different affinity for the ammonia molecules.

Additional conclusions can be derived from the temperature of the peak maximum in the ammonia TPD tests (T_{max}). The value corresponding to the ordered mesoporous materials is quite lower than those of the zeolite samples pointing out the weaker acidity of the former. While the T_{max} of the two ordered mesoporous materials is quite similar, important variations are observed in the zeolite samples. As it occurred with the acid sites concentration, the position of the peak maximum is gradually lowered as the ratio external/micropore surface area is increased. Both trends suggest that the hierarchical zeolites possess an overall weaker acidity compared with the reference one, which would imply that the acid strength of the sites located on the mesopore external surface is lower than that of the acid sites confined inside the zeolite micropores. However, it must be taken into account that NH_3 may be not the best molecule for probing the acidic properties of materials having different types of acid sites. Therefore, the acidic properties of these materials have been also investigated by adsorption–desorption of other bases in order to distinguish and isolate the contributions of Brønsted and Lewis acid sites.

FTIR spectroscopy in combination with probe molecules of different sizes and basicity is one of the best methods to characterize acid sites in molecular sieves, particularly when hierarchical materials are under study [42]. Pyridine, 2,6-di-tert-butylpyridine and d_3-acetonitrile are the most frequently employed probe molecules. Their application allows qualitatively as well as quantitatively to describe the type of acid sites, their concentration and also the acid strength of individual acid centres [43–45]. The region of hydroxyl groups in the infrared spectra of zeolites or other aluminosilicate

materials consists of three different types of OH group vibrations: (i) silanol groups at 3745 cm^{-1}, characteristic of terminal silanols, and silanol groups at 3732 cm^{-1} inside zeolitic defaults (or the string of interacting with each other silanol groups); (ii) bands between 3610 and 3620 cm^{-1} corresponding to bridging acidic Si–OH–Al groups, and (iii) a wide absorption band centred around 3500 cm^{-1}, ascribed to the presence of species having hydrogen atoms in a weak hydrogen bond, detected when zeolite crystallites are defect rich (silanol nests).

Fig. 6 depicts the FTIR spectra in the hydroxyl region of zeolite samples after activation in vacuum at 450 °C. It is worth to note that the absorption band around 3500 cm^{-1} was not observed in these zeolites. Thus, it can be inferred that no hydroxyl nests or hydrogen bonds of bridging OH groups with silanols are present, confirming a high quality and ordering of the structure of these zeolites [46].

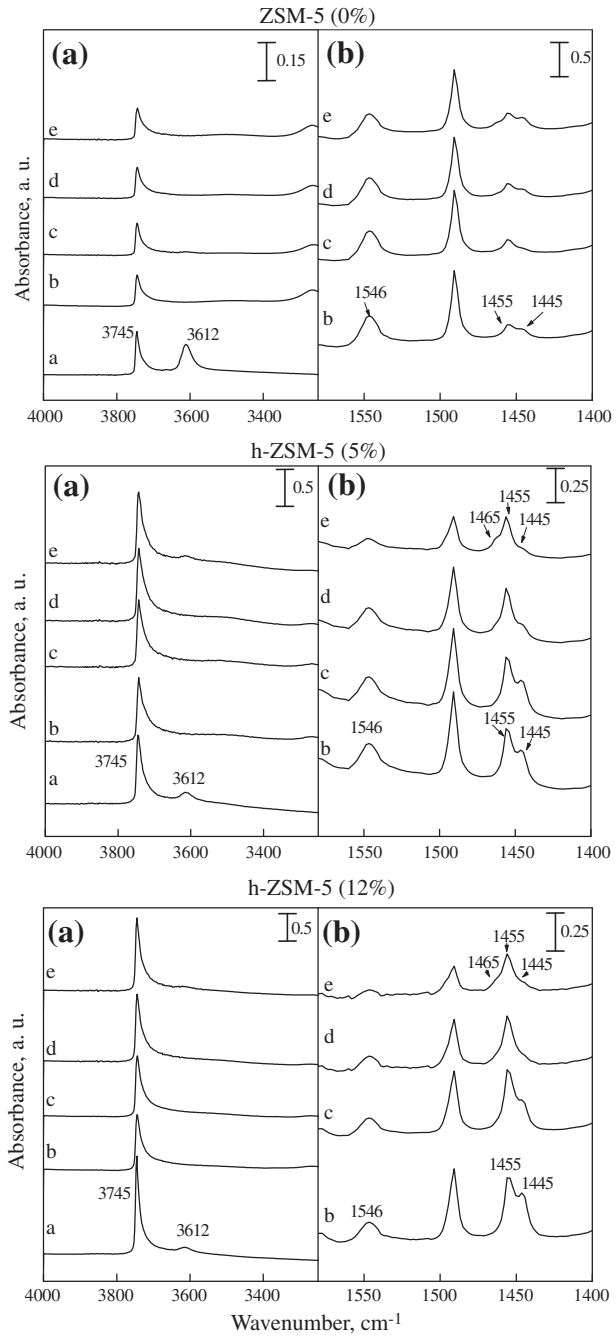

Fig. 6. FT-IR spectra of the ZSM-5 samples after pyridine adsorption: (a) spectra of activated samples; (b) after 20 min desorption 150 °C; (c) 250 °C; (d) 350 °C; (e) 450 °C.

The FTIR spectra recorded after adsorption of excess pyridine and its consecutive desorption carried out at different temperatures are shown in Fig. 6. ZSM-5 zeolites, independently of the synthesis procedure, exhibit two absorption bands at 3745 and 3612 cm^{-1}. The former band is due to non-acid silanol groups, while the latter one is assigned to acidic bridging Si–OH–Al groups. After pyridine desorption at 150 °C, the band at 3612 cm^{-1} disappears due to the interaction with pyridine. Further desorption steps at 250 and 350 °C did not lead to re-appearance of this band evidencing the strong interaction of pyridine with Brønsted acid sites and confirming their high acid strength. Pyridine desorption at 450 °C led to a partial re-appearance of this band. It clearly shows that most Brønsted sites of the zeolite still retain adsorbed pyridine molecules even at high temperatures.

In contrast, Fig. 7 shows that the infrared spectra of Al-MCM-41 and HZM do not exhibit a band of bridging Si–OH–Al groups. The absence of this band is a typical feature for MCM-41-type materials. In the case of HZM, this fact could indicate a low concentration of zeolitic units in the sample or the presence of Al atoms forming mainly Lewis acid sites.

Pyridine adsorption on the different samples leads to the appearance of new absorption bands corresponding to pyridine interacting with Brønsted (1545 cm^{-1}) and Lewis acid sites (1445–1465 cm^{-1}). In all materials studied, a band at 1545 cm^{-1} is visible, although its intensity strongly depends on the sample. Relatively high intensities were obtained for all ZSM-5 zeolites for the band at 1545 cm^{-1}, its intensity being slightly decreased with the desorption temperature. Both Al-MCM-41 and HZM samples also exhibit a low-intensity band at this wavenumber, indicating a possible existence of pyridine complexes adsorbed on Brønsted acid sites in spite of the above commented absence of the band corresponding to acidic Si–OH–Al groups in their original spectra. Two or even three absorption bands were observed in the area of pyridine bands interacting by electron donor bonds with Lewis acid sites (1445–1465 cm^{-1}). The absorption band at 1445 cm^{-1} is commonly assigned to pyridine interacting with silanol groups. This band usually re-appears after desorption performed at 250 °C or even 350 °C. With all ZSM-5 samples, after desorption at 450 °C, a new band around 1462 cm^{-1} appears in the spectra. Recently, this phenomenon was described for zeolite SSZ-35 based on the combined effect of pyridine migration and "in situ" formation of strong Lewis sites [14].

Fig. 8 provides for the different samples the concentrations of Brønsted and Lewis acid sites determined after pyridine desorption in the range between 150 and 450 °C. The reference ZSM-5 (0%) is the material with the highest concentration of Brønsted sites, while this value is significantly lower for the hierarchical ZSM-5 samples. The opposite is observed for the Lewis acid sites, showing high concentrations in the hierarchical zeolites. In fact, for these samples the concentration of Lewis sites is higher than that of Brønsted sites for most of the desorption temperatures. Interestingly, this Lewis acid is quite strong as denoted by the high concentration of Lewis sites observed even after pyridine desorption at 450 °C in the hierarchical ZSM-5 samples.

Regarding the ordered mesoporous materials, both Al-MCM-41 and HZM show little pyridine adsorbed on Brønsted sites, although with a higher concentration for the hybrid ordered mesoporous material. In contrast, these samples exhibit high concentrations of Lewis sites. In the case of Al-MCM-41, this concentration decreases strongly with the pyridine desorption temperature. However, for HZM, the behaviour is completely different as the concentration of Lewis sites remains very high even after desorption at high temperatures. These results indicate that both hierar-

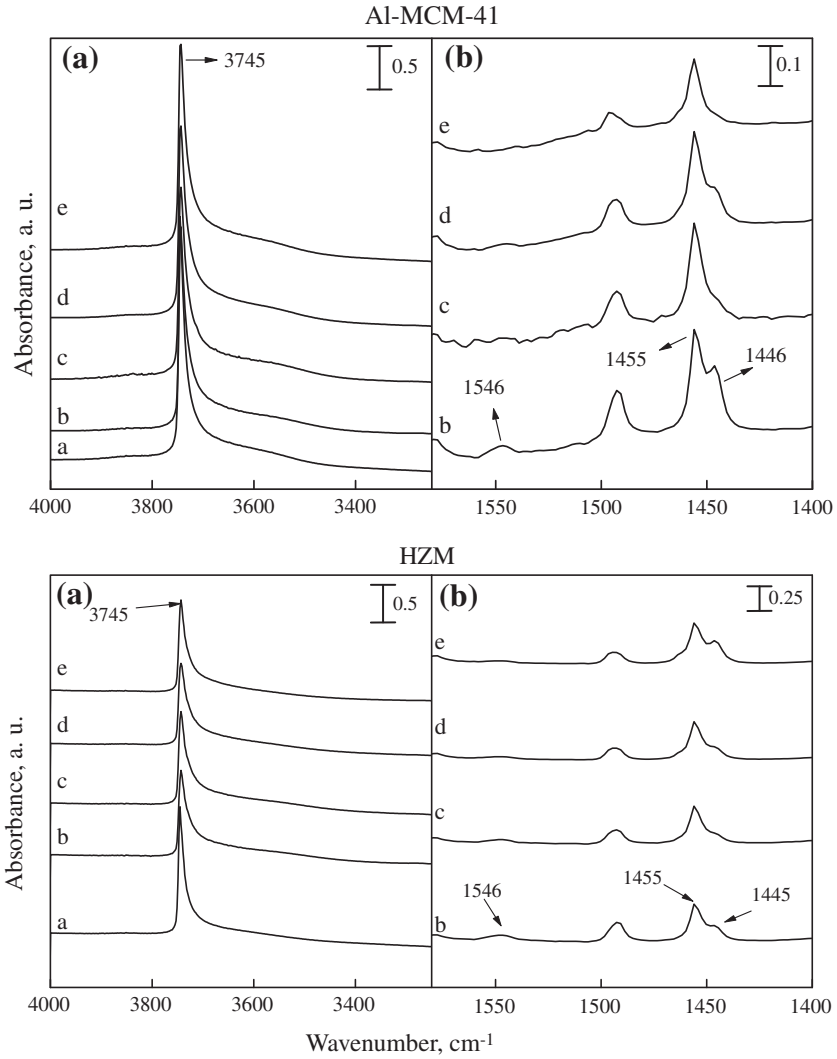

Fig. 7. FT-IR spectra of the ordered mesoporous material samples after pyridine adsorption: (a) spectra of activated samples, (b) after 20 min of desorption 150 °C; (c) 250 °C; (d) 350 °C; (e) 450 °C.

chical ZSM-5 and HZM samples have in common the presence of strong Lewis acid sites.

The acidic properties of the materials studied were also investigated by adsorption of d_3-acetonitrile. Acetonitrile is a small molecule, which can diffuse easily in the zeolite channels. In addition, its basicity is lower than that of pyridine, which allows the different acid sites to be better distinguished. Fig. 9 shows the FTIR spectra of the samples after d_3-acetonitrile adsorption–desorption. The d_3-acetonitrile adsorption leads to the formation of new bands at 2300 cm^{-1}, originated from the interaction with Brønsted sites, and at 2325 cm^{-1}, caused by interaction with Lewis acid sites.

Quantitative evaluation of the concentration of both types of acid centres, derived from d_3-acetonitrile adsorption, is given in Fig. 10. Clear differences are visualized when hierarchical zeolites are compared with the ZSM-5 (0%) sample used as reference. Thus, an inversion in the area under peaks involved, i.e. 2300 and 2325 cm^{-1}, is visibly detected. Therefore, a significant shift from Brønsted to Lewis acid takes place for hierarchical zeolites, which agrees well with the pyridine adsorption results, previously stated, despite the different basicity and kinetic diameters of both probe molecules. Likewise, for the ordered mesoporous materials, the results of d_3-acetonitrile adsorption confirm that the acid sites present in both Al-MCM-41 and HZM are mainly of Lewis type, whereas just a small amount of Brønsted sites is detected in both cases.

When comparing hierarchical zeolites and ordered mesoporous materials, location of acid sites can play an important role. Based on that, 2,6-di-tert-butylpyridine was also used as probe molecule to discriminate the acid sites at the non-microporous surfaces of the samples because its diameter prevents its adsorption inside the 10 rings of the MFI zeolitic structure. After the adsorption of 2,6-di-tert-butylpyridine, the formation of a new absorption band at 1530 cm^{-1} is observed (see Supporting information, Fig. S3). The absence of the band at 1545 cm^{-1} evidences that no dealkylation of 2,6,-di-tert-butylpyridine occurs. Small concentrations of Brønsted acid sites determined by 2,6-di-tert-butylpyridine sorption prove that only sites located at the mesopore/external surface of the materials are evaluated. On the other hand, adsorption of 2,6-di-tert-butylpyridine leads to substantial differences among the individual samples, which are consistent with the type of materials under study. Thus, while 2,6-di-tert-butylpyridine is practically not adsorbed on conventional ZSM-5 (0%) sample, significant intensities were obtained for hierarchical h-ZSM-5 (5%) and h-ZSM-5 (12%) materials since this bulky molecule is able to diffuse into the mesopores of the hierarchical samples. Finally, the highest concentrations of acid sites on the mesopore/external

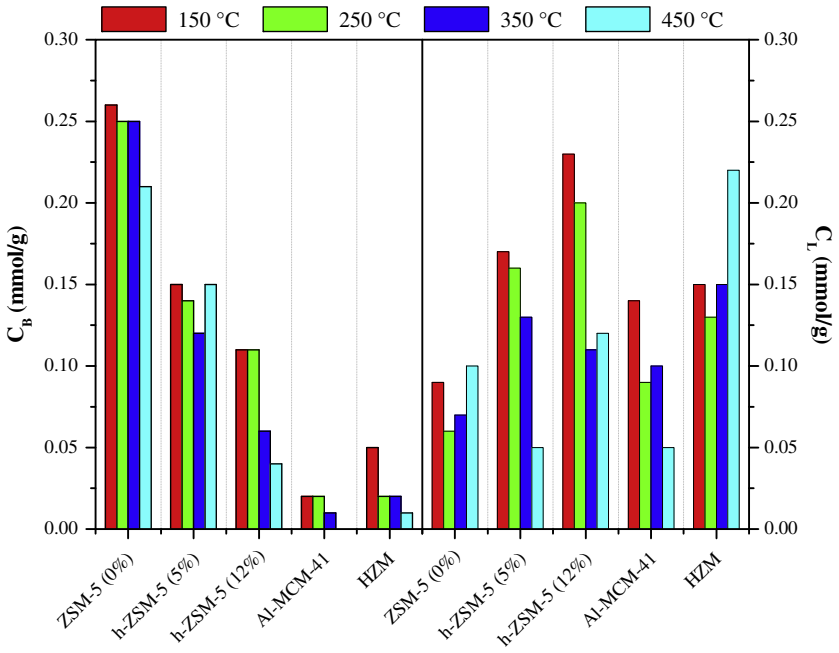

Fig. 8. Concentration of Bronsted (C_B) and Lewis (C_L) acid sites in the samples measured by FTIR/pyridine adsorption at different temperatures.

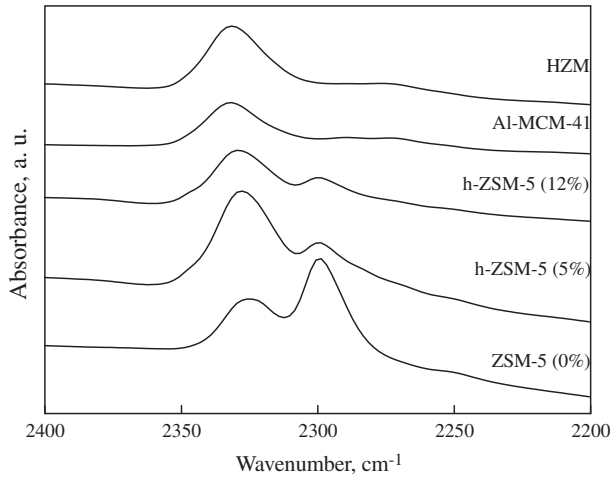

Fig. 9. FT-IR spectra of the samples after 30 min of acetonitrile adsorption–desorption at room temperature.

surface were achieved for Al-MCM-41 and HZM, where the acid sites are mainly located at the mesopores surface.

3.5. Catalytic properties for 1,2-epoxyoctane rearrangement

Isomerisation of 1,2-epoxyoctane, catalysed by both Brønsted and Lewis acids, is an attractive reaction to test the catalytic properties of the different materials studied in this work, since it is expected to be very sensitive to their different textural and acidic properties as they may exert a considerable influence over both the catalytic activity and the product distribution.

The epoxide isomerization reaction in the presence of Lewis and Brønsted acid sites begins with the oxirane ring cleavage, which subsequently may progress through different pathways, resulting in the formation of a variety of compounds (see Scheme 1), such as 1,2-octanediol (II), 2-octanone (III), octanal (IV), 2-octen-1-ol (V), 3-octen-1-ol (VI) and 2-butyltetrahydrofuran (VII) [30]. From an industrial point of view, the most important products coming from the 1,2-epoxyoctane isomerisation are octaldehyde (IV) and monounsaturated alcohols (V and VI), since they are employed as intermediates in fine chemistry. Additionally, secondary reactions may occur as a result of the aldol condensation of octenol [47].

Fig. 11a shows the evolution of the epoxide conversion along the reaction time obtained with the different acidic catalysts studied. The reference ZSM-5 (0%) sample displays the lowest conversion, while very high values are exhibited by the ordered mesoporous materials. Thus, 100% epoxide conversions are achieved over the latter catalyst after just 1 h of the reaction time. An intermediate behaviour is observed for the hierarchical ZSM-5 samples with a remarkable improvement in the conversion regarding the reference ZSM-5, although with values still lower than those of the ordered mesoporous materials. These results denote a high significance of the accessibility to the active sites for this reaction, which explains the excellent catalytic activity of the two ordered mesoporous materials and the improvement achieved with the hierarchical ZSM-5. Nevertheless, the nature of the acid sites is probably also an important factor in determining the catalytic activity. Although the contribution of the Brønsted acidity cannot be completely neglected, the Lewis acid sites seem to play the most important role in catalysing the 1,2-epoxyoctane rearrangement. Thus, the highest conversion is obtained with the HZM sample, which is the material possessing the best combination of accessibility (non-microporous surface area) and concentration of strong Lewis acid sites.

Important differences are observed between the catalysts in terms of product distribution. Fig. 11b shows the product selectivity corresponding to the different catalysts after 30 min and 2 h of reaction time. The main products formed over the reference ZSM-5 (0%) sample are 1-octaldehyde and octenols, being obtained in similar proportions. In addition, small amounts of other products are also produced with this catalyst (around 3 mol%), mostly including heavy compounds formed by aldol condensation of the above-mentioned primary products. For the hierarchical ZSM-5 samples, a moderate increase in the selectivity towards heavy products takes place (8–10 mol%), which seems to be enhanced with the external surface area of these materials. This effect occurs

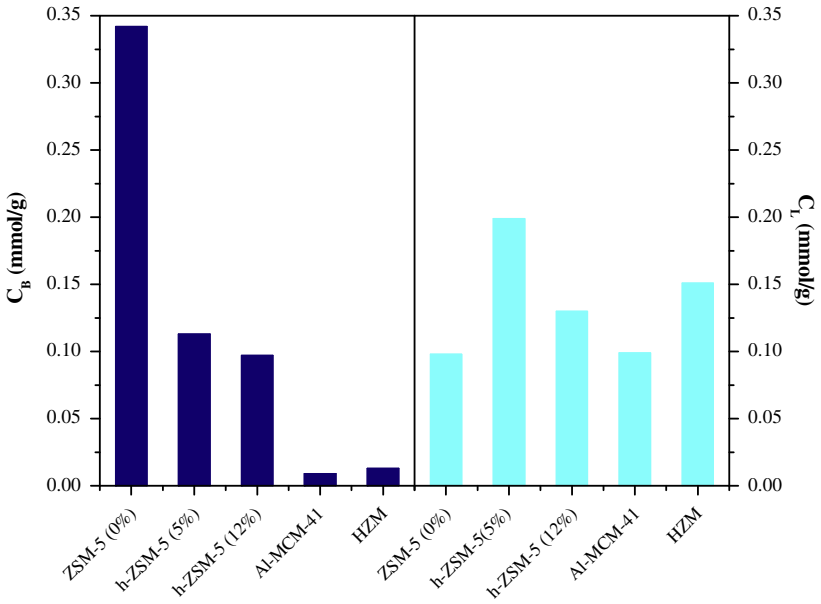

Fig. 10. Concentration of Bronsted (C_B) and Lewis (C_L) acid sites in the samples measured by FTIR/acetonitrile adsorption–desorption at room temperature.

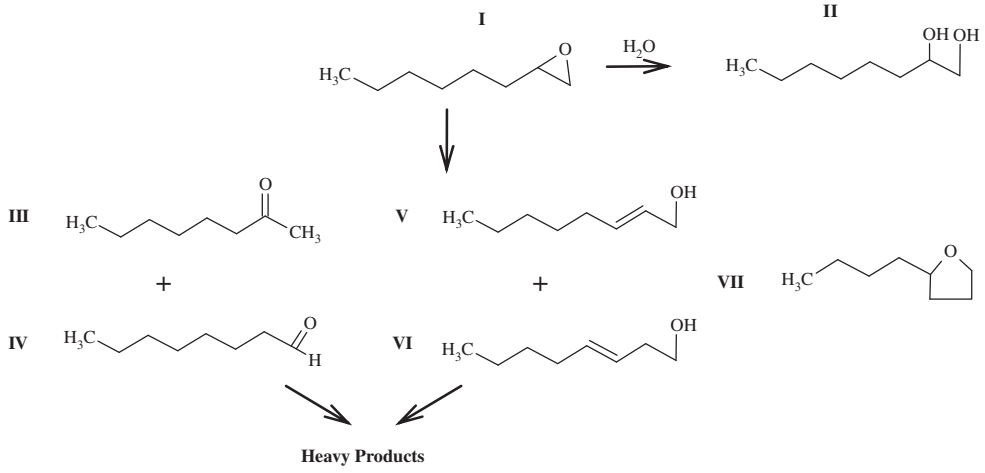

Scheme 1. Isomerization of 1,2 epoxyoctane (I) to obtain 1,2-octanediol (II), 2-octanone (III), octanal (IV), 2-octen-1-ol (V), 3-octen-1-ol (VI) and 2-butyltetrahydrofuran (VII).

mainly in detriment of the octenols, while the octanal selectivity is kept almost constant, showing that the former are the main compounds participating in aldol condensation reactions over the hierarchical zeolites. Regarding the ordered mesoporous materials, some differences between them are clearly visualized. After 30 min of the reaction, Al-MCM-41 is selective towards the octanal formation, while HZM material promotes the aldol condensation reactions. These results may be explained taking into account the differences in the reaction rates observed at short reaction times for both materials. HZM presents a steeper slope than Al-MCM-41, and accordingly a faster reaction rate. Both the higher number and the different types of acid sites that HZM possesses seem to accelerate the formation of heavy compounds even at such short times. However, at longer reaction times (2 h), the formation of heavy products is clearly enhanced over both HZM and Al-MCM-41, becoming the main products obtained over ordered mesoporous catalysts, 58 and 47 mol%, respectively. Accordingly, aldol condensation is also clearly promoted by the catalysts having a high Lewis acidity and absence of steric and diffusion limitations.

3.6. Catalytic properties for anisole acylation

The catalytic behaviour of both hierarchical zeolites and hybrid mesoporous-zeolitic materials has been also investigated for anisole acylation using acetyl chloride as acylating agent [21]. This is an interesting reaction since, as shown in Scheme 2, it leads to the formation of p-methoxyacetophenone (p-MAP) having applications in fine chemistry.

Fig. 12 illustrates the anisole conversion as a function of the reaction time using the different catalysts. For all them, p-MAP was obtained almost as the only product with a selectivity over >97%. Blank experiments, run without catalyst under the same conditions, did not show any conversion of anisole. With all the catalysts, the anisole conversion reaches a plateau at 180 min of reaction. Since both reactants are still present in the reaction medium, this fact indicates that all catalysts could suffer an inhibition process by reaction products, as consequence of the adsorption/desorption equilibrium, which is in agreement with previous literature works using this type of materials [48]. Inhibition in this sys-

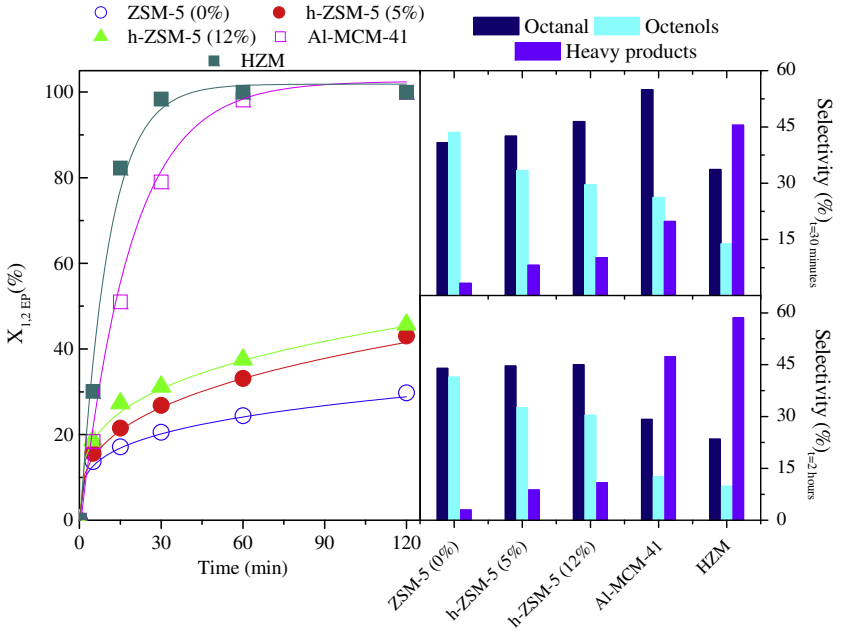

Fig. 11. Behaviour of the different catalysts on 1,2-epoxyoctane isomerization: (a) conversion, (b) product distribution at 30 min and (c) product distribution at 2 h.

Scheme 2. Acylation of anisole.

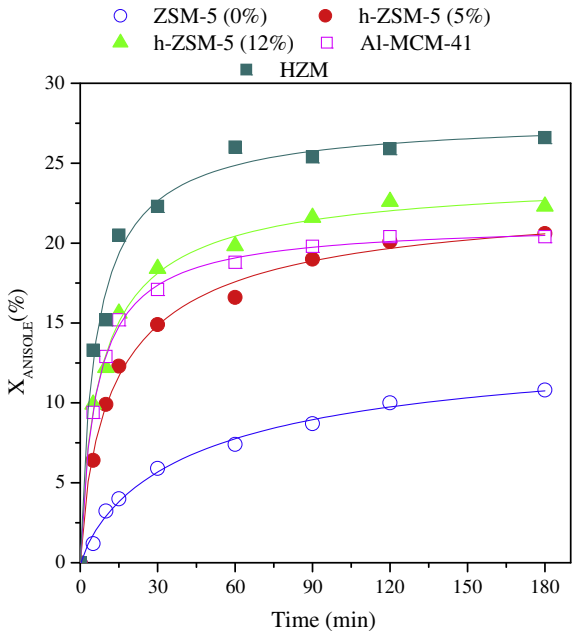

Fig. 12. Behaviour of the different catalysts on anisole acylation.

tem has been assigned mainly to the strong adsorption of p-MAP on the actives sites, which produces a competition with the adsorption of the reactants, since the equilibrium adsorption constant for the p-MAP product is several times higher than those of anisole and acetyl chloride [21,49]. The direct consequence is that the reaction product remains strongly adsorbed on the active sites, hindering the access and interaction of the reactants with these acid sites.

In the case of conventional ZSM-5 (0%), the anisole conversions obtained were remarkably lower than those on other catalysts, reaching at best a 10% value. This is probably due to the relatively small size of the ZSM-5 micropores compared with those of anisole and p-MAP, which causes diffusion and steric limitations for this reaction to be catalysed by the active sites located within the zeolite microporosity. In contrast, the anisole conversion is quite higher when using hierarchical ZSM-5 samples as catalysts. Thus, h-ZSM-5 (5%) shows enhanced reaction rates and conversions than the reference zeolite sample. A small, but still noticeable, increase in both the reaction rate and anisole conversion is also observed when going from h-ZSM-5 (5%) to h-ZSM-5 (12) samples. At a first glance, this may be interpreted as a direct consequence of the presence of hierarchical porosity in these materials, reducing the diffusion hindrances for the reaction and providing also a significant amount of external surface area, which is expected to show no steric restrictions. Nevertheless, the effect of the changes in the acid features introduced by the hierarchical porosity should be also taken into account. As above discussed, hierarchical ZSM-5 samples possess a high content of strong Lewis acid sites, which are expected to catalyse also the anisole acylation.

In the case of the ordered mesoporous materials, the catalytic activity and conversion obtained over the HZM sample were higher than those corresponding to the Al-MCM-41 material, showing that also for this reaction, the presence of zeolitic fragments within the mesopore walls improves their catalytic properties.

Finally, if the behaviour of both zeolites and ordered mesoporous materials is compared, it is concluded that the latter exhibit a higher activity as it occurred in 1,2-epoxyoctane isomerization.

However, in this case, the differences are less important. Thus, h-ZSM-5 (12%) sample leads, at long reaction times, to 22.3% anisole conversion, i.e. slightly higher than that of Al-MCM-41 (20.4%), probably due to its higher resistance to inhibition by p-MAP adsorption. This is a really interesting fact since standard ZSM-5 is considered not to be a good catalyst for anisole acylation.

In summary, these results confirm that the combination of a good accessibility and strong Lewis acidity in both hierarchical ZSM-5 and hybrid zeolitic/ordered mesoporous materials strongly improves their catalytic properties compared with reference samples in reactions suffering of diffusion and/or steric limitations, as it is the case of aromatic Friedel–Crafts acylation.

4. Conclusions

Two different strategies for obtaining MFI zeolite-based materials with high accessibility starting from protozeolitic units are compared. The first one is based on perturbing their aggregative growth by grafting of organosilanes, which leads to hierarchical ZSM-5. The second one consists in the controlled assembly of the protozeolitic units around surfactant micelles to form hybrid ordered mesoporous materials (HZM).

Hierarchical ZSM-5 samples present a secondary porosity in the mesopore range, which causes great changes in their textural properties leading to both enhanced BET and non-microporous surface areas. However, this causes also a slight reduction in the stability of the Al species during calcination and a lowering of the acid strength. Strong changes are observed in the nature of the acid sites as a consequence of the generation of a secondary porosity. Hierarchical ZSM-5 samples posses a high concentration of Lewis acid sites, which is in contrast to the predominant Brønsted nature in the reference ZSM-5 sample. Interestingly, as denoted by the FTIR spectra of pyridine adsorbed on the samples, these Lewis sites are very strong, retaining adsorbed pyridine at high temperatures.

The presence of MFI nanounits in the HZM sample cannot be directly probed as this material is X-ray amorphous. Likewise, no microporosity is detected in this sample when analysing the nitrogen adsorption isotherm, probably because the width of the mesopore walls is too small to accommodate MFI units with micropores. However, ^{27}Al MAS NMR measurements indicate a higher uniformity and stability of the Al atoms in the HZM material compared with the reference Al-MCM-41 sample, which is consistent with MFI fragments being present within the pore walls. Moreover, investigation into the acidic properties by adsorption–desorption of different bases show that HZM possesses a larger concentration of Brønsted acid sites than Al-MCM-41, whereas it exhibits also a stronger Lewis acidity as observed for the hierarchical ZSM-5. These results confirm the hybrid nature of the HZM sample.

The variation of the textural and acidic properties of the materials has a strong effect on their catalytic activity for 1,2-epoxyoctane rearrangement and anisole acylation.

The results obtained in 1,2-epoxyoctane isomerization show the high significance of the accessibility to the active sites, which explains the excellent activity of the two ordered mesoporous materials and the improvement achieved with the hierarchical ZSM-5. Nevertheless, the nature of the acid sites probably also plays an important factor in determining the catalytic activity. Although the contribution of the Brønsted acidity cannot be completely neglected, the Lewis acid sites seem to play the most important role in catalysing the 1,2-epoxyoctane rearrangement. The main products formed over the reference ZSM-5 sample are the octanal and octenols, being obtained in similar proportion. For the hierarchical ZSM-5 samples, a moderate increase in the selectivity towards heavy products takes place, which seems to be enhanced with the external surface area of these materials. The formation of heavy products is even more favoured over the ordered mesoporous materials, becoming the main products obtained with both HZM and Al-MCM-41. Accordingly, this secondary reaction is also clearly promoted by the catalysts having a high Lewis acidity and being free of steric and diffusional limitations.

In the case of anisole acylation to yield p-MAP, the results obtained confirm that the combination of a good accessibility and strong acidity in both hierarchical ZSM-5 and hybrid zeolitic/ordered mesoporous materials significantly improves their catalytic properties compared with reference samples. Thus, both reaction rates and anisole conversion are quite higher in hierarchical ZSM-5 samples compared with standard ZSM-5, whereas a remarkable increase in the value of these parameters is also denoted when comparing HZM with Al-MCM-41.

Acknowledgment

The financial support of the Spanish government (CTQ2005-09078/PPQ and CTQ2008-05909/PPQ) is gratefully acknowledged.

Appendix A. Supplementary data

Supplementary data associated with this article can be found, in the online version, at doi:10.1016/j.jcat.2011.02.007.

References

[1] J. Coronas, Chem. Eng. J. 156 (2010) 236.
[2] C.T. Kresge, M.E. Leonowicz, W.J. Roth, J.C. Vartuli, J.S. Beck, Nature (1992) 359.
[3] A. Taguchi, F. Schüth, Micropor. Mesopor. Mater. 77 (2005) 1.
[4] R.M. Martin-Aranda, J. Čejka, Top. Catal. 53 (2010) 141.
[5] J. Čejka, S. Mintova, Catal. Rev. 49 (2007) 457.
[6] K. Egeblad, Christina H. Christensen, M. Kustova, C.H. Christensen, Chem. Mater. 20 (2008) 946.
[7] D.P. Serrano, J. Aguado, J.M. Escola, J.M. Rodriguez, A. Peral, Chem. Mater. 18 (2006) 2462.
[8] R. Srivastava, M. Choi, R. Ryoo, Chem. Commun. 43 (2006) 4489.
[9] L. Tosheva, V.P. Valtchev, Chem. Mater. 17 (2005) 2494.
[10] J.C. Groen, W. Zhu, S. Brouwer, S.J. Huynink, F. Kapteijn, J.A. Moulijn, J. Perez-Ramırez, J. Am. Chem. Soc. 129 (2007) 355.
[11] A. Karlsson, M. Stocker, R. Schmidt, Micropor. Mesopor. Mater. 27 (1999) 181.
[12] M. Choi, K. Na, R. Ryoo, Chem. Commun. 20 (2009) 2845.
[13] N. Žilková, M. Bejblová, B. Gil, S.I. Zones, A.W. Burton, C.Y. Chen, Z. Musilová-Pavlačková, G. Košová, J. Čejka, J. Catal. 266 (2009) 79.
[14] B. Gil, S.I. Zones, S.J. Hwang, M. Bejblová, J. Čejka, Phys. Chem. C 112 (2008) 2997.
[15] V.V. Ordomsky, V.Y. Murzin, Y.V. Monakhova, Y.V. Zubavichus, E.E. Knyazeva, N.S. Nesterenko, I.I. Ivanova, Micropor. Mesopor. Mater. 105 (2007) 101.
[16] M.S. Holm, S. Svelle, S. Joensen, P. Beato, C.H. Christensen, M. Bjoergen, Appl. Catal. A 356 (2009) 23.
[17] J. Perez-Ramirez, C.H. Christensen, K. Egeblad, C.H. Christensen, J.C. Groen, Chem. Soc. Rev. 37 (2008) 2530.
[18] D.P. Serrano, J. Aguado, J.M. Escola, J.M. Rodriguez, A. Peral, J. Mater. Chem. 18 (2008) 4210.
[19] P. Prokesova, N. Zilkova, S. Mintova, T. Bein, J. Cejka, J. Appl. Catal. A 281 (2005) 85.
[20] Y. Liu, W. Zhang, T.J. Pinnavaia, Angew. Chem. Int. Ed. 40 (2001) 1255.
[21] D.P. Serrano, R.A. Garcia, D. Otero, Appl. Catal. A 359 (2009) 69.
[22] R.A. Garcia, D.P. Serrano, D. Otero, J. Anal. Appl. Pyrolysis 74 (2005) 379.
[23] N.S. Nesterenko, F. Thibault-Starzyk, V. Montouillout, V.V. Yuschenko, C. Fernandez, J.-P. Gilson, F. Fajula, I.I. Ivanova, Micropor. Mesopor. Mater. 71 (2004) 157.
[24] E.J. Creyghton, J.A. Elings, R.S. Downing, R.A. Sheldon, H. van Bekkum, Micropor. Mater. 5 (1996) 299.
[25] F. Thibault-Starzyk, I. Stan, S. Abello, A. Bonilla, K. Thomas, C. Fernandez, J.-P. Gilson, J. Pérez-Ramírez, J. Catal. 264 (2009) 11.
[26] M. Trombetta, T. Armaroli, A. Gutierrez-Alejandre, J. Ramirez, G. Busca, Appl. Catal. A 192 (2000) 125.
[27] A. Corma, V. Fornes, L. Forni, F. Marquez, J. Martinez-Triguero, D. Moscotti, J. Catal. 179 (1998) 451.
[28] J. March, Advanced Organic Chemistry: Reaction, Mechanism and Structure, sixth ed., Wiley-Interscience, New Jersey, 2007, p. 1599.
[29] K. Arata, K. Tanabe, Catal. Rev. Sci. Eng. 25 (1983) 365.
[30] D.P. Serrano, R. van Grieken, J.A. Melero, A. García, Appl. Catal. A 269 (2004) 137.
[31] G.A. Olah, Friedel-Crafts and Related Reactions, Wiley-Interscience, New York, 1973.
[32] P. Botella, A. Corma, M.T. Navarro, F. Rey, G. Sastre, J. Catal. 217 (2003) 406.

[33] R.A. Sheldon, H. van Bekkum, Fine Chemical through Heterogeneous Catalysis, Wiley-VCH, Weinhein, 2000.
[34] G. Sartori, R. Maggi, Chem. Rev. 106 (2006) 1077.
[35] M. Guidotti, C. Canaff, J.-M. Coustard, P. Magnoux, M. Guisnet, J. Catal. 230 (2005) 375.
[36] E. Fromentin, J.-M. Coustard, M. Guisnet, J. Catal. 190 (2000) 433.
[37] U. Freese, F. Heinrich, F. Roessner, Catal. Today 49 (1999) 237–244.
[38] R. van Grieken, J.L. Sotelo, J.M. Menéndez, J.A. Melero, Micropor. Mesopor. Mater. 39 (2000) 135.
[39] A. Matsumoto, H. Chen, K. Tsutsumi, M. Grün, K. Unger, Micropor. Mesopor. Mater. 32 (1999) 55.
[40] R.A. García, D.P. Serrano, G. Vicente, D. Otero, M. Linares, Stud. Surf. Sci. Catal. 174 (2008) 1091.
[41] E. Oldfield, J. Haase, K.D. Schmitt, S.E. Schrammb, Zeolites 14 (1994) 101.
[42] J. Datka, B. Gil, A. Kubacka, Zeolites 17 (1996) 428.
[43] A. Corma, V. Fornes, L. Forni, F. Márquez, J. Martínez-Triguero, D. Moscotti, J. Catal. 179 (1998) 451.
[44] S. Zheng, H.R. Heydenrych, A. Jentys, J.A. Lercher, J. Phys. Chem. B 106 (2002) 9552.
[45] Z. Musilová-Pavlačková, S.I. Zones, J. Čejka, Top. Catal. 53 (2010) 273.
[46] B. Gil, Ł. Mokrzycki, B. Sulikowski, Z. Olejniczak, S. Walas, Catal. Today 152 (2010) 24.
[47] D. Brunel, M. Chamoumi, P. Geneste, P. Moreau, J. Mol. Catal. A 79 (1993) 297.
[48] D. Rohan, C. Canaff, E. Fromentin, M. Guisnet, J. Catal. 177 (1998) 296.
[49] E.G. Derouane, I. Schmidt, H. Lachas, C.J.H. Christensen, Catal. Lett. 95 (2004) 13.